Modeling & Simulation of Aerodynamic Flow Around NACA-4421 Airfoil

– Assignment 1 2023

Tarun Teja, (tarna588)
Abhishek Dhiman, (abhdh352)

LINKÖPINGS UNIVERSITET

Linköping University
Division of Applied Thermodynamics and Fluid Mechanics
Scientific Report

1 Introduction

In many engineering applications, modeling and simulation have become foundation stones and are widely used for Aerodynamic studies. Knowledge from air-flow dynamics merged with a computational approach to evaluate the flow around objects with optimal configurations and boundary conditions are utilized to replicate the physical phenomena. This saves time for experimental setup and expenses leading to significant research in developing turbulence models in the CFD domain.

Selection of NACA-4421 is motivated by the intriguing thickness of the airfoil, preferred for low-speed flying to achieve high lift at low angles of attack (α). It is also good for small remote-controlled airplanes for short take-off, landing, and ease of wing construction. The Reynolds number and experimental data for validation purpose is based on the study [1]. The analysis of NACA-4421 airfoil for both viscid and inviscid flow is performed using Xfoil tool for Reynolds No. (R_e) = 3110000 [1]. The viscid flow analysis is conducted in Ansys Fluent for three methods, namely, Spalart-Allamaras, k-ω SST (Shear Stress Transport) and $\gamma - R_{e_\vartheta}$ transition SST. The range of (α) $\in$ [–8° to 30°] is selected to study the behaviour of various models for this complex flow and highlighting the limitations of these models. The Transition γ - Re_ϑ SST (TSST) model is also employed to study the transition from laminar to turbulent or vice-versa which also gets captured by the Xfoil.

The fundamental objective of this assignment/study is to explore the strengths and weaknesses of panel methods and compare them with popular turbulence models available in ANSYS Fluent (R2 2022). To briefly explore the transition estimation by TSST and comment on the under-lying assumptions. Eventually, the comparison of merits, demerits, and limitations of above mentioned models from Fluent and Xfoil (based on panel methods) at low-speed incompressible flow with boundary conditions.

2 Methodology

2.1 Mesh and Boundary conditions

The Xfoil program provides design and analysis capabilities of existing airfoil with interactive design. Both, viscous and inviscid analysis cab be performed, with forced and free transition prediction and lift-drag predictions near α_{cr} for all airfoils. The program is based upon the higher order panels method and computationally very in-expensive. The lift coefficient (C_l) calculation is performed by direct integration of surface pressure and for drag coefficient (C_d) Squire-Young formula with the underlying assumption of asymptotic wake behaviour downstream of point of application. The handling of the transition point in Xfoil is done by e^N criterion for free transition due to linear instability which happens to be the case with majority of airfoil applications. The Xfoil program contains the airfoil database of existing airfoils from which NACA4421 with chord length of 1 [m] is used to obtain the results. The range of (α) $\in$ [–8° to 30°] is selected to study the strength (α_{cr} <= 14°) and weaknesses (α_{cr} => 14°) in the behaviour captured by Xfoil for the complex flow. Three panel sizes [100, 300, 500] with α increment of 2° in the mentioned range for both viscous and inviscid modes at R_e = 3110000. The panel sizes are varied to obtain grid convergence for lift and drag coefficients, and the analysis of free transition behaviour.

The next set of data comes from the ANSYS Fluent (R2 2022) using various RANS models and is compared against Xfoil data. The coordinates of the selected NACA-4421 airfoil is generated using Airfoil Tools [2] with 200 points (max) with a chord length of 1 [m]. The coordinates are saved in txt/csv file with a standard 5-column format supported by the ANSYS design modeler.

An unstructured mesh with triangular elements is used with edge sizing of 500 divisions on the airfoil curve, Fig. 1. Essentially, 25 inflation layers with a first layer thickness of (0.01 [mm]) to achieve $y^+ < 1$ are applied in the airfoil. The inflation growth rate = 1.1 to resolve the boundary layer and viscous sub-layer. The sphere of influence has played a vital role in achieving significant mesh refinement and aid in resolving gradients of governing equations in the area of interest.

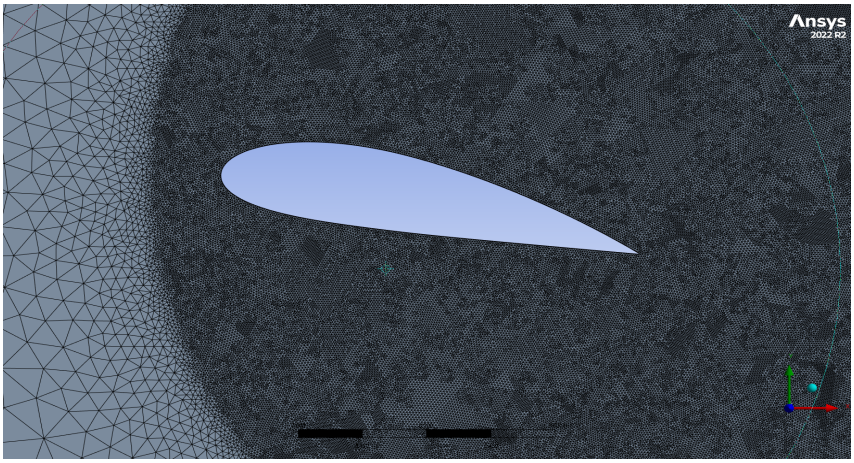

Figure 1: Domain mesh with body of influence at $\alpha = 12^\circ$

Boundary condition at the inlet side is such that to obtain $R_e = 3110000$ with air as fluid medium [1] and for the outlet side pressure-outlet is applied with zero gauge pressure. The top and bottom sides of the domain have symmetry condition as the boundary are sufficiently far from the airfoil. The airfoil curve accounts for the wall with the no-slip condition. For the domain influence and mesh verification he $k-\omega$(SST) turbulence model is used with low Re-correction to damp high the turbulent viscosity [3] in the viscous sub-layer at the wall. Hybrid initialization is performed for better convergence. Standard initialization was observed to give oscillations during residual convergence. In fluent, the pressure-based solver is used since the flow conditions are subsonic and incompressible. Coupled scheme is employed for pressure-velocity coupling to enhance the rate of convergence significantly as it solves the momentum and pressure equations together [4]. The time scale factor is [0.5], and second-order schemes for the pressure and momentum equation are employed.

The domain size influence simulation are performed for a rectangular domain around the airfoil for different domain sizes [7c, 11c, 13c, 15c, 17c, 19c] with k-ω SST model at $\alpha = 12^\circ$, Fig. 2. The domain size is crucial to prevent influences of outer boundary on the body of interest, hence determination of a good domain size is also part of this study. The c_d and c_l deviation obtained for 15c domain compared to 19c domain is 2.176 % and 1.39 % respectively. For domain size below 15c the deviation is more that 5%, hence for mesh verification and further analysis 15c domain size is opted.

2.2 Mesh Verification

The grid independence study is performed to achieve the grid convergence for c_d and c_l with the 15c domain size and $\alpha = 12^\circ$, Fig. 3. 5 meshes (M1-M5) are created out of which 3 meshes (M1, M3, M4) are utilized with($r > 1.33$) [5] for Gird Convergence Index (GCI) calculation. The GCI calculation and other parameter values are shown in Table.1 based on which Mesh4

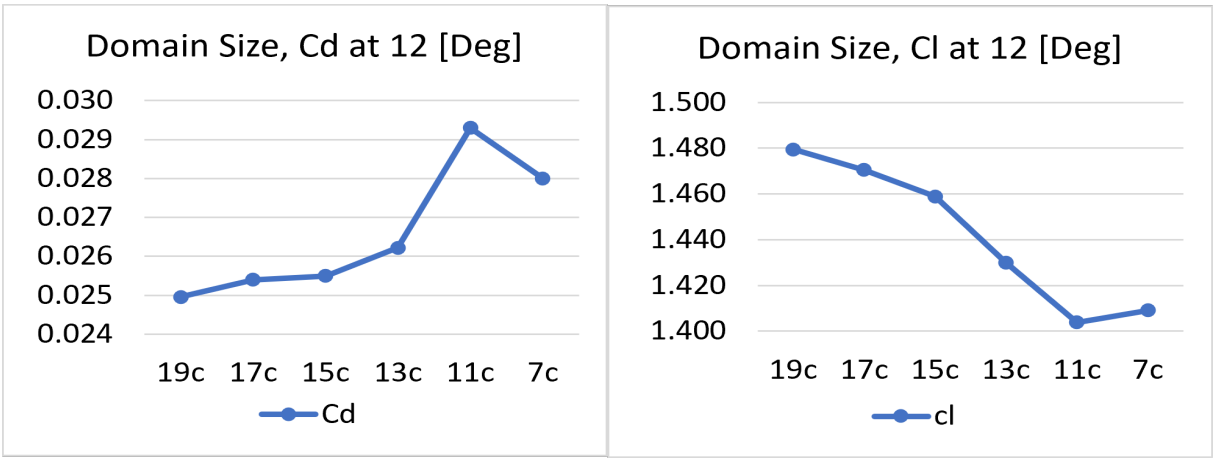

Figure 2: Domain size influence study for c_l and c_d at $\alpha = 12°$

(M4) is selected for further analysis with GCI below 10% and also the convergence commences at M4, Fig. 3. The % error of M4 w.r.t M5 for output parameters c_l and c_d is 0.6 % and 2.21 % respectively, hence making M4 a good choice.

Table 1: Mesh Verification and Grid Convergence Index (GCI), $\alpha = 12°$

Mesh	Nodes	Elements	h_{value}	r_{GR}	c_l	c_d	GCI(c_l%)	GCI(c_d)%
M1	31648	59630	124.88	-	1.177	0.041	-	-
M2	97864	188839	70.17	1.78	1.366	0.031	13.614	22.306
M3	198968	387926	48.96	1.433	1.442	0.027	9.205	8.576

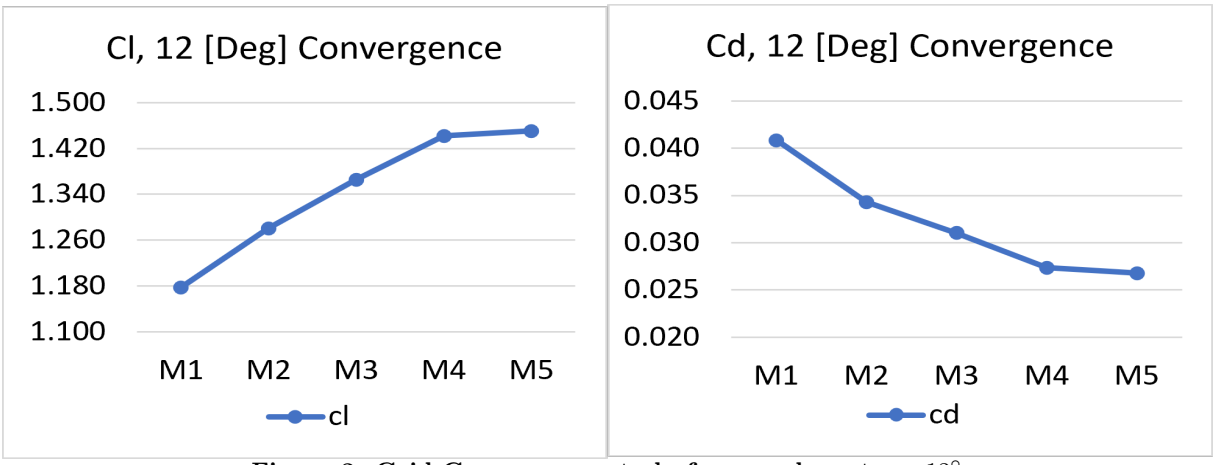

Figure 3: Grid Convergence study for c_l and c_d at $\alpha = 12°$

3 Results

The Xfoil and CFD results are plotted for c_l comparison for α range of $[(-8)° \longrightarrow 32°]$ in Fig. 5. The results from Xfoil were obtained for panel numbers (100, 300, 500) for convergence in viscid and inviscid flows, Fig. 4. For the inviscid flow case, the c_l increase is linear with α as the flow is completely attached over the airfoil as there is no shear stress and hence no drag forces. On the other hand, the loss of lift force due to the viscous effects are seen in Fig. 4 for $\alpha > 14°$ which is also observed in [1].

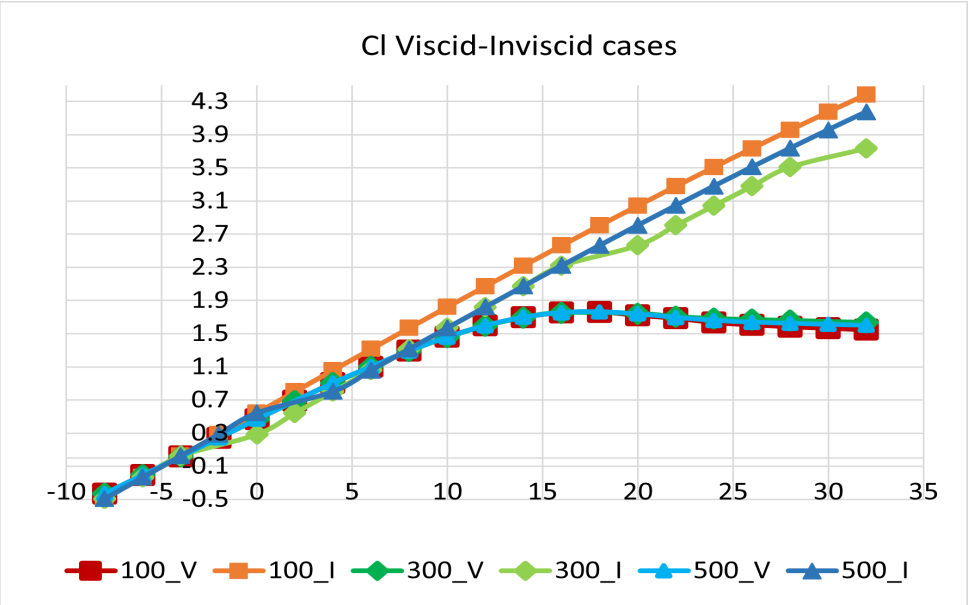

Figure 4: c_l **vs** α **for viscous (V) & Inviscid (I) Xfoil for No. of panels** $\in$ **[100, 300, 500]**

Upon comparison of c_l and c_d obtained from Xfoil against RANS models like Spalart-Allamaras (SA), k - ω SST (SST) and γ - $Re_{\vartheta,t}$ Transition SST (TSST), a good agreement is observed till $\alpha <= 14°$, Fig. [5a, 5b]. Near the critical angle ($\alpha_{cr} = 14°$), the influence of flow separation is well captured by the RANS models (SST and SA) compared to Xfoil showing sharp decline in c_l and sharp rise in c_d slopes, Fig. 5. On the other hand, all three panels (100, 300, and 500) with viscous Xfoil mode show no significant lift loss (c_l) Fig. 5a and fairly constant. For drag rise (c_d) Fig. 5b for increment prediction by Xfoil almost half SST and SA.

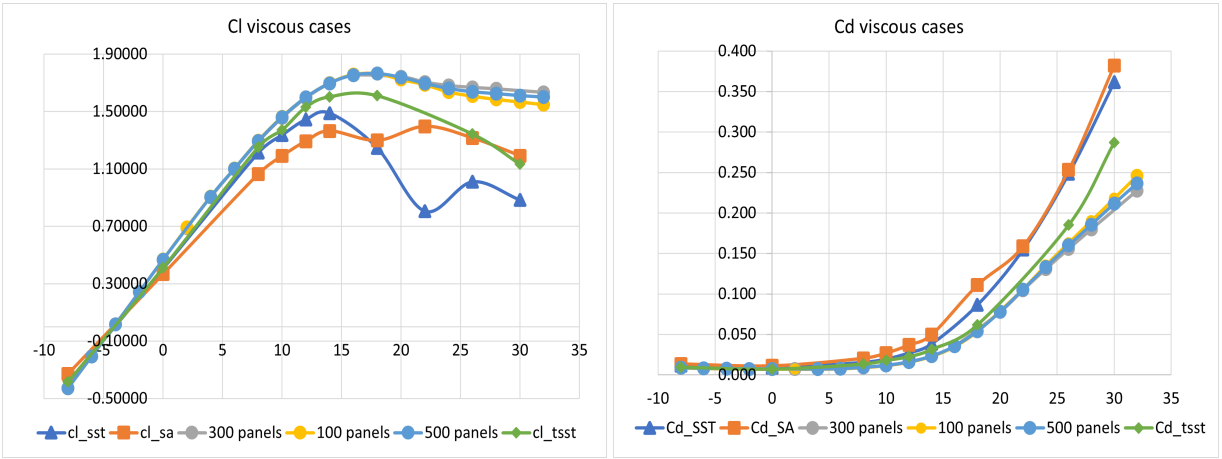

(a) c_l **viscous comparison between RANS and Xfoil** **(b)** c_d **viscous comparison between RANS and Xfoil**

Figure 5: c_l **and** c_d **for RANS models and Xfoil (No. of panels** $\in$ **[100, 300, 500])**

The one-equation model **Spalart - Allamaras** (SA) is based on the kinematic eddy viscosity parameter that works well for external flow physics, specially developed for resolving pressure gradient in the boundary layer. The SA model shows closest agreement to SST (alpha $<= 14°$) but slightly under-predicts the c_l value whereas for $\alpha => 22°$ the agrees well with TSST, Fig. 5a. On the other hand, the c_d curve of SA is in complete agreement with SST over the entire range of α with marginal deviations for $14° <= \alpha <= 22°$, Fig. 5b.

The γ - $Re_{\vartheta,t}$ **Transition SST** model solves 2 additional equation for γ (intermittency) - $Re_{\vartheta,t}$ (transition Re). For c_l, a significant deviation is observed at $\alpha_{cr} = 14$ and follows close trend with Xfoil results, Fig. 5a. The c_d values agree well with Xfoil c_d values and start to deviate for $\alpha > 22°$, Fig. 5b. The intermittency contour in Fig. 6a shows the building up of fluctuations on the top and bottom airfoil accounting for transition. The intermittency chart in

Fig. 6b, quantifies the increase in γ at 0.25c (bottom) and 0.4c (top) airfoil edges implying the transition on the surface. The complete turbulence has not been achieved as intermittency ($\gamma < 1$) is very small at $\alpha = 0$, probably signifying the formation of small disturbances due to increase in pressure gradient along airfoil curve.

The pressure coefficient (c_p) plots (Fig. [7a, 7b, 7c]) and skin friction coefficient (c_f) (Fig. [7d, 7e, 7f]) for three RANS models at ($\alpha_{cr} = 14°$, $\alpha = 18°$, $\alpha = 26°$) are shown respectively. At $\alpha_{cr} = 14°$ all three models show similar results of pressure distribution but as the α increases the flow separation point tends to move towards the leading edge (from 0.6c to 0.2c). For the skin friction distribution the TSST model shows two peak values where the 1st peak grows with α and 2nd peak remains steady for the suction surface of airfoil. The SST peak values grow gradually whereas the SA peak C_f value growth is drastic showing maximum value at $\alpha = 18°$ and $\alpha = 26°$ compared to SST and TSST.

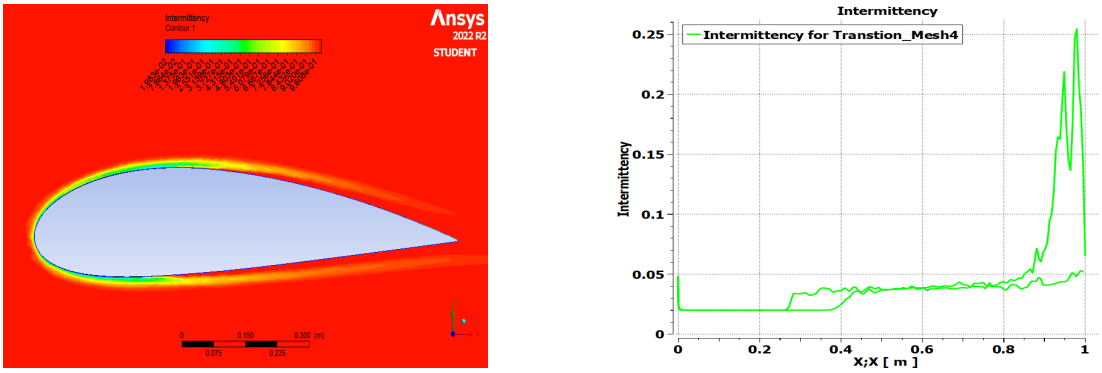

(a) Intermittency Contour at $\alpha = 0$ **(b) Intermittency chart at $\alpha = 0$**

Figure 6: The intermittency capturing the % time the turbulent fluctuation in the boundary layer.

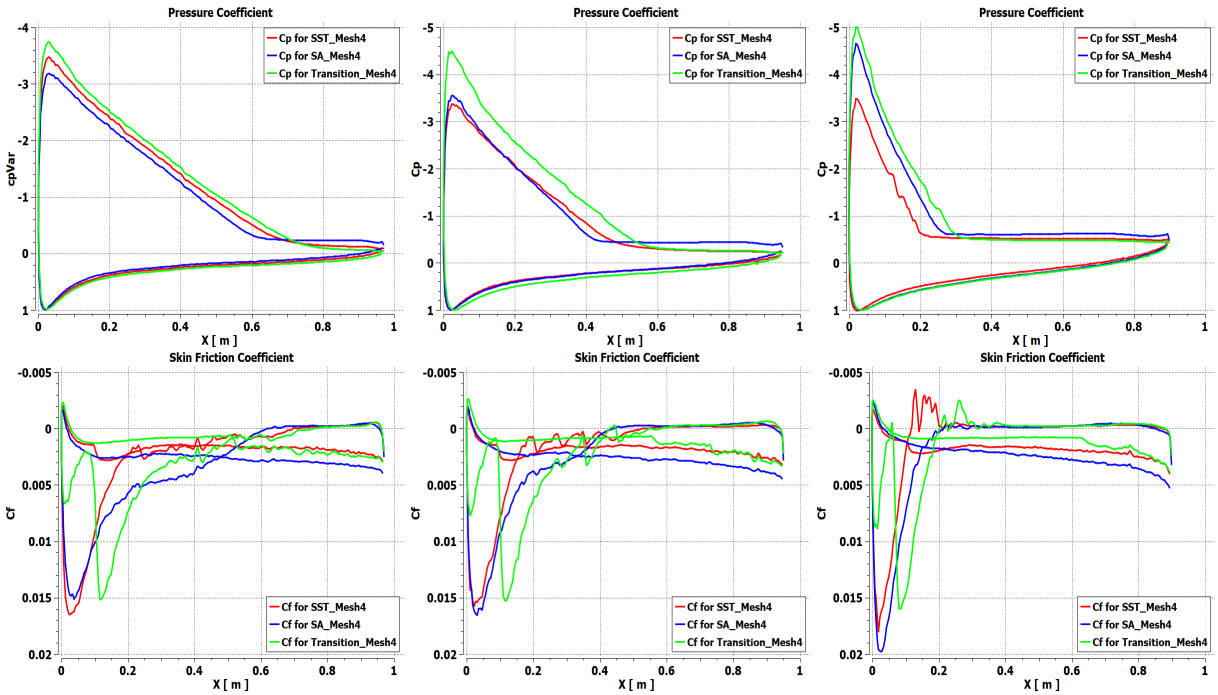

(d) C_f at $\alpha = 14$ **(e) C_f at $\alpha = 18$** **(f) C_f at $\alpha = 26$**

Figure 7: Pressure coefficient (c_p) and skin friction coefficient (c_f) at $\alpha \in [14°, 18°, 26°]$

The pressure peak for the SST model remains the same but SA and TSST is over-estimated. The highest c_p estimates are shown by the TSST model in all three cases. The SA model estimate increases rapidly, i.e overlapping with SST at $\alpha = 18°$ Fig. 7b to overlapping with TSST at $\alpha = 18°$ Fig. 7c.

4 Discussion

The Xfoil c_l curves for viscous flow showed good inclinations to the RANS models upto $\alpha_{cr} = 14°$ with over-prediction if $c_{l_{max}}$ values compared to RANS models and also highlighted the limitation of capturing lift loss due to the flow separation for $\alpha_{cr} > 14°$ Fig. 5a. The lack of modeling of eddy viscosity in panel methods highlights the inability to capture the viscous sub-layer, boundary layer and flow separation influence on c_l (over-prediction) and c_d (under-prediction) [6]. The promoting the reliability of RANS models at α_{cr} and slightly above it. The c_d curve of Xfoil and **Spalart-Allamaras (SA)** model is in great agreement, Fig. 5b since the SA model lacks sensitivity towards rapidly changing flow such as airfoil wake and complex flow near critical AoA. Hence failing to capture the transport properties well compared to other RANS models [7], clearly seen as SA deviations for c_d and c_l for α in [15° to 22°] Fig. 5.

The RANS models showed great similarities as expected over the entire range of α but with a few limitations in resolving wake region. The SA model is based on the kinematic eddy viscosity parameter (linear in viscous sub-layer) and works well for external flows [7]. The wall damping function of this model becomes 1 for high R_e and 0 at the wall [7]. But compared to the SST model it lacks the ability to resolve the various mixing lengths of the wake region and mostly is limited to predetermined mixing lengths based on the log-law [7] leading to poor agreement between SST and SA model for c_l ($\alpha > 14°$) and c_d ($14° <= \alpha <= 22°$). The eddy viscosity modelling of SST model and underlying merits of k-ε away from wall and k-ω near wall region controlled by the blending function are main strengths of SST [3]. Therefore, making SST highly reliable for flows such as adverse pressure gradient for α well below α_{cr} because when α comes closer to α_{cr} or greater the transient physics and significant separation needs to be considered which lowers the SST reliability.

Next is the TSST model, solving for intermittency (γ) and Transition R_e ($Re_{\vartheta,t}$) compared to the SST model. The calculation of gamma allows getting an estimate of transition by setting $\gamma = 0$ in the laminar boundary layer, $\gamma = 1$ in the fully turbulent boundary layer, and $0 < \gamma < 1$ in the transition zone, Fig. 6b. This basically tells the percentage of time that the turbulent fluctuations are present in the boundary layer. The critical momentum thickness R_e ($Re_{\vartheta,c}$) where the intermittency first starts to increase and the transition zone length both are empirically related to ($Re_{\vartheta,t}$) [8].

The stability of SST model compared to SA and TSST for ($14° <= \alpha <= 26°$) adverse pressure gradient well know and seen in Fig. 7. The pressure peak value remains for the same and the flow separation point moves towards the leading edge with increasing α capturing the practical aspect of highest c_l at $\alpha_{cr} = 14°$. Similarly, the C_f rise is gradual for SST and TSST out performing the SA model for separated flow. The 1st C_f peak shown by TSST in Fig. 7 implies the C_f rises as the intermittency (γ) increases with α. This lack of stability make TSST and SA comparatively, less trust worthy than SST for C_p estimation, whereas only SA is less reliable in case of C_f.

5 Conclusions

The study of flow around NACA-4421 using XFoil and various turbulence models is performed to estimating the strengths and weaknesses of each model. The performances are analysis on various parameters like change in lift and drag coefficients with α and the pressure distribution behaviour for α above critical value. The domain domain size influence study gave important insights about the consideration and acceptable error limits while selecting the domain size. The

following conclusion are derived based on the presented work.

- The domain size 15c is the smallest size resulting in discretization error below 5% for both c_d an c_l.
- The critical angle (α_{cr}) for NACA 4421 is estimated to be 14° by all the models used in the study showing good agreement with experimental data [1].
- All the models used in present study showed good agreement for $\alpha <= 14°$.
- The strengths of SST model for complex steady flow with adverse pressure gradient is well predicted by c_l and c_d curve, along with pressure and skin friction distribution over the airfoil.
- The transition capturing ability of TSST model showed trade-off with c_d, c_l and pressure peak estimations.
- The SA model built to capture external flow lacks the resolution provided by SST model.
- The lack of viscous modeling in Xfoil restricts its application to completely laminar flows and preliminary analysis.

References

[1] Jacobs Eastman N Ward RM Kenneth E Pinkerton. The characteristics of 78 related airfoil sections from tests in the variable-density wind tunnel. December 20 1932.

[2] Airfoil coordinates;. Available from: `http://airfoiltools.com/airfoil/naca4digit`.

[3] Shear-Stress Transport (SST) k- ω Model;. Available from: `https://www.afs.enea.it/project/neptunius/docs/fluent/html/th/node67.htm`.

[4] Pressure-Velocity Coupling;. Available from: `https://www.afs.enea.it/project/neptunius/docs/fluent/html/th/node373.htm`.

[5] et al IBC. Procedure for Estimation and Reporting of Uncertainty Due to Discretization in CFD Applications. 2008.

[6] Why Use a Panel Method;. Available from: `https://www.symscape.com/blog/why_use_panel_method`.

[7] Vesteeg HK, Malalasekera W. An Introduction to Computational Fluid Dynamics. 4th ed. Pearson Education LTD; 2007.

[8] Transport Equations for the Transition SST Model;. Available from: `https://www.afs.enea.it/project/neptunius/docs/fluent/html/th/node74.htm`.